Design and implementation of a capacitive leaf wetness sensor based on capacitance to digital conversion

Design and implementation of a capacitive leaf wetness sensor based on capacitance to digital conversion

Elena Filipescu, Giovanni Paolo Colucci and Daniele Trinchero, *Member, IEEE,*

***Abstract*—An innovative implementation of an electronic leaf wetness sensor (LWS) is proposed. It utilizes capacitive sensing, combined with an innovative data acquisition method, which implements a capacitance-to-digital converter. The study explores the design procedure of a capacitive LWS, proposing an analytical approach and emphasizing low manufacturing costs. Since the LWS is intended for Internet of Things (IoT) applications, the paper estimates its energy consumption, introducing a boost regulator to optimize power usage, contributing to extend the battery life. The study presents simulation results and experimental validations, including an ad-hoc calibration procedure in controlled conditions. The sensors were tested in real agricultural environments over a complete vegetative season, demonstrating their capability to operate continuously without problems.**

***Index Terms*—Fungal infections, leaf wetness, capacitive leaf wetness sensor, energy saving, IoT, capacitance-to-digital converter.**

I. Introduction

In agriculture, for a large variety of crops, the presence of water on the leaf surface, identified as "leaf wetness", mainly due to humidity, fog, rainfall and excessive irrigation, may cause several diseases [1]. To protect the crops, it is important to regularly monitor it. Leaf wetness duration (LWD), which is the sum of each single wetness period that occurs between two dry intervals [2], is crucial for the development of fungal infections. A leaf wetness sensor (LWS), able to monitor, possibly in real time, the leaf wetness, is essential to predict and prevent plant diseases. Moreover, combining the sensor with any of the several transmission methods available for the Internet of Things (IoT), it is possible to massively deploy the device to finally characterize any real scenario.

II. State-of-the-art

Among already existing LWSs technologies, static and mechanical sensors have been used since the 1950s [2], [3]. The majority of them only allow to assess whether a leaf is dry or wet [4]. Moreover, they are suitable only for visual observation and cannot be implemented in a circuit. They are easy to use, but they lack in robustness, and consequently they are not suitable for automatized measurements.

LWD can be indirectly measured as the period during which the difference between the effective temperature and the dew point is below a predefined threshold [5]. To this purpose, the detection can be carried out by means of Stevenson screens hosting temperature and humidity sensors, the dew point being function of temperature and relative humidity, according to approximate formulations like the Bosen's one [6].

In the last 20 years, electronic sensors have been introduced and, thanks to versatility and smaller dimensions, have been increasingly used [2], [7].

Electronic LWSs allow direct measurements. Two alternatives exist:

- resistive, using two metallic conductors, usually gold plated, whose ohmic resistance changes in presence of humidity [3];
- capacitive, measuring the dielectric constant of the material between two electrodes, which varies if water is present on the surface of the sensor [8].

Both simulate the behavior of a real leaf and are characterized by stability and reliability; capacitance ones are more efficient [9], but also more expensive [7].

In the recent years, an alternative solution based on a microwave approach has been proposed; unfortunately, it cannot be applied to the IoT because it requires higher energy provisioning [10].

More recently, our group has presented an innovative capacitive sensor, tested in field for short periods [11]. In the present paper, we propose a complete design procedure for the device. Additionally, considering the sensor's potential applications in the IoT domain, we include an extra section that evaluates the sensor energy consumption. Finally, we provide long-term validation in field.

III. Proposed solution

An electronic sensor suitable for IoT applications is proposed, with the following characteristics:

- low production costs, allowing large or dense deployments;
- minimal power consumption, allowing use with any IoT platform;

This work was partially supported by PSR 2014-2020, Regione Piemonte, Operazione 16.1.1, "Integrated Tools for the Environmental Sustainability of the Vineyard" (SISAV) Project (CUP J66B20006500002); the European Union under the Italian National Recovery and Resilience Plan (PNRR) of Next-GenerationEU, partnership on "Telecommunications of the Future" (PE00000001 - program "RESTART") and the Agritech National Research Center (PNRR – MISSIONE 4 COMPONENTE 2, INVESTIMENTO 1.4 – D.D. 1032 17/06/2022, CN00000022). This manuscript reflects only the authors' views and opinions, neither the European Union nor the European Commission can be considered responsible for them.

The authors are with the Department of Electronics and Telecommunications, Politecnico di Torino, 10129 Torino, Italy (email: elena.filipescu@polito.it; giovanni.colucci@polito.it; daniele.trinchero@polito.it).

- repeatable and reliable measurements, allowing any agronomic exploitation.

To this aim, a capacitive solution has been chosen, implementing an innovative data acquisition method, based on use of capacitance-to-digital converters (CDCs), inexpensive and easy to find off the shelf. Compared to the majority of available commercial solutions, which are based on voltage measurements, the one selected reduces power consumption. Finally, capacitance-based sensors guarantee adequate precision, typical of this category of LWSs.

The usage of a CDC requires a conditioning circuit specifically dimensioned to perform the measurement in the correct range. In our case, the capacitance under measurement, the conditioning circuit and the CDC are integrated on the same board, differently from what is found in literature [7, 8], where reading circuit and the conditioning circuit are external. For this purpose, to optimize the sensor configuration and to provide an operational instrument for the correct design of the conditioning circuit, an analytical procedure for a preliminary computation of the sensor capacitance has been introduced.

A. Design of the Sensing Subsystem

To design the sensing subsystem, we opted for a customized solution, instead of an off-the-shelf one, in order to integrate it on the same printed circuit board (PCB) that hosts the data acquisition subsystem.

As the majority of the commercial devices do, the sensing subsystem consists of a two-sided capacitive leaf wetness sensor. We decided to use a circular geometry of radius R. On each surface, the capacitance is synthesized with $2N+1$ parallel horizontal metallic strips, the odd ones connected to a central vertical one, the even ones connected to an external strip aligned along the circumference (Figure 1a and Figure 1b).

Each leaf side is modeled as a set of N coplanar waveguides with finite-sized ground planes, repeated symmetrically on the left and on the right (Figure 1b). The model is studied with the waveguide immersed in two different media: air ($\epsilon_r = 1$) and water ($\epsilon_r = 78.57$ [12]). The model does not take into account the presence of three different media, as in the typical case of a surface treated with solder mask, but this does not represent a significant limitation, as it is shown later.

Four conductors (`A`, `B`, `C`, `D`) form each line i. Line $i+1$ uses conductor `C` of line i as `B`, while the ground plane (`D`) is unique for all lines (Figure 2).

Each line i, independently of the fact that the two terminals are taken on opposite sides, because of its relative shortness, is equivalent to a standard transmission line of length l_i, terminated in open circuit. The input admittance for each line is:

$$Y_i = \frac{1-\cos 2kl_i + j\sin 2kl_i}{1+\cos 2kl_i - j\sin 2kl_i}\sqrt{\frac{C_{tl}}{L_{tl}}} \tag{1}$$

where C_{tl} and L_{tl} are, respectively, capacitance and inductance per length unit of the transmission line i, recomputed according to [13], where the upper half-space capacitance depends on the dielectric constant of the surrounding medium ϵ_{rm}:

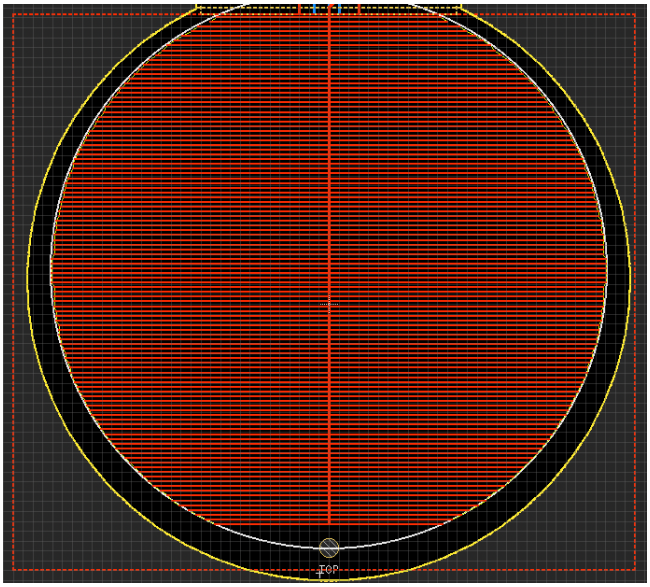

(a) PCB schematics

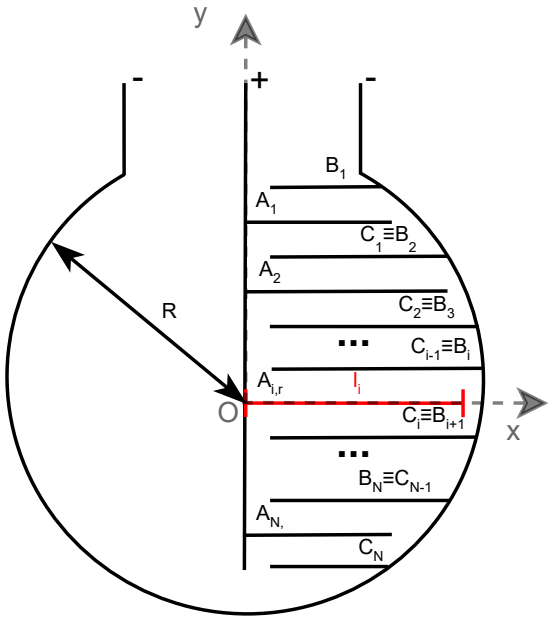

(b) Strips pattern

Figure 1: Sensing surface configuration [11]

$$C_{tl} = 2\epsilon_0\left[\epsilon_{rm}K(k)/K(k') + \epsilon_r K(k_1)/K(k_1')\right] \tag{2}$$

$$L_{tl} = \frac{\mu_0}{2}\frac{1}{K(k)/K(k') + K(k_1)/K(k_1')} \tag{3}$$

where K is the complete elliptic integral of the first kind and the propagation indexes are defined as follows:

$$k_1 = \frac{tanh[\pi w/4h]}{tanh[\pi(w+2s)/4h]} \tag{4}$$

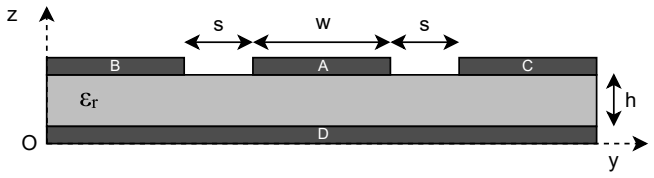

Figure 2: Grounded coplanar waveguide model of the upper leaf

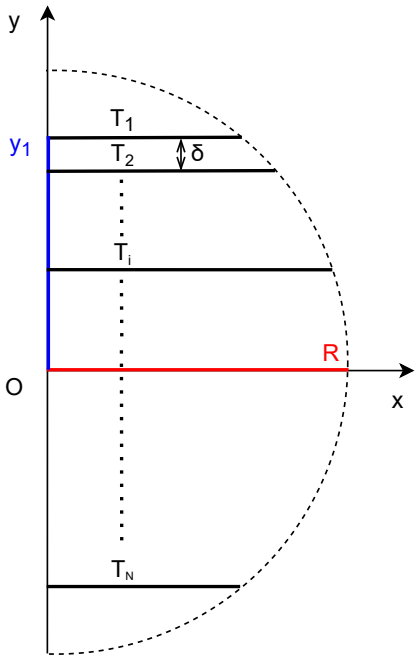

Figure 3: Geometrical modeling of line l_i

$$k = \frac{w}{w + 2s} \tag{5}$$

$$k_1'^2 = \sqrt{(1 - k_1^2)} \tag{6}$$

Typical leaf dimensions are $h \sim 0.1\,\text{mm}$, $s \sim 0.15\,\text{mm}$, $w \sim 0.15\,\text{mm}$, $l_i < 5\,\text{cm}$. According to [13], with these dimensions, the transmission line is almost equivalent to a capacitance, being $\omega L l << 1/(\omega C l)$, independently of the frequency value, which belongs to the range 10 kHz - 10 MHz for almost all CDCs.

Being $l_i \ll \lambda$, the arguments of $\cos 2kl_i$ and $\sin 2kl_i$ are negligible, thus $Y_i = j\omega C_{tl} l_i$. The sensor admittance is then computed as the sum of each line input admittance Y_i, consequently, the total sensor capacitance is:

$$C_{tot} = 2C_{tl} \sum_{i=1}^{N} l_i \tag{7}$$

where l_i is the transmission lines length:

$$l_i = \sqrt{R^2 - \Big(y_1 - (i-1)\delta\Big)^2} \tag{8}$$

according to Figure 3, where each symbol T_i represents schematically the whole line i, y_1 is the distance from center of line 1 and $\delta = 2(w + s)$.

In this multimodal structure, three modes propagate [14]: a non-TEM slotline, and two quasi-TEM microstrip and coplanar, respectively.

In order to maintain a mono-modal excitation with a dominating coplanar waveguide behavior, the following excitation tricks were adopted [15]:

1) the slotline mode excitation is avoided by keeping the two side components (B, C) at the same electric potential;
2) the microstrip mode excitation, is avoided by keeping the lower ground plane (D) and the two upper side ground planes (B, C) at the same potential.

B. Design of the Data Acquisition Subsystem

We chose to construct the data acquisition subsystem using the FDC2x1x family of CDCs from Texas Instruments, which are multi-channel, noise- and EMI-resistant, high-resolution and high-speed, supporting a wide excitation frequency range, which offers flexibility in system design. This family of chips is widely available on the market, indeed the same technology is used for the common capacitive touchscreen of mobile phones and watches and the specific FDC2x1x chips are used for many technology applications based on capacitive sensing solutions [16]. CDC allows to keep both cost and power consumption low. Moreover, the supply voltage ranges from $2.7\,\text{V}$ to $3.6\,\text{V}$, in a lower interval, compared to the one in $[5 - 18]\text{V}$ used by several capacitive LWSs. This range of voltage levels is better applicable to a variety of microcontrollers.

Since LWSs require a maximum of two independent measurements, respectively for the upper and lower leaf side, two channels are sufficient, so the FDC2112 was chosen.

Other CDCs were evaluated but not selected, as the primary objective was to minimize the energy consumption. For example, FDC1004 [17] has a standby mode of 29 μA, against the shutdown mode of 200 nA in FDC2112. This last device was consequently chosen, being in low power mode during the majority of the time.

Differently from traditional switched-capacitance architectures, the chosen CDC measures the oscillation frequency of an L-C resonator. The FDC2x1x employs an L-C resonator as a sensor, thus a change in capacitance of the L-C tank corresponds to a shift in the resonant frequency. The value of the capacitance is obtained through an indirect measurement: the device outputs a digital value, proportional to frequency, which can be converted to an equivalent capacitance.

In the typical measurement configuration, the unknown capacitance is connected only to IN0A, while INxA and INxB are connected through an L-C conditioning circuit.

In the proposed configuration, as it is shown in Figure 4, the L-C circuit that connects the INxA-INxB is by itself the object of the measurement, with the inductor constant and the capacitor equal to the capacitive leaf face plus a constant offset, introduced to optimize the frequency range.

The sensor capacitance C_{SENS} is computed using (9), where L_c and C_c are the components of the conditioning circuit for channel x. Their values must be set by taking

into account that the sensor excitation frequency ranges from 10 kHz to 10 MHz. Hence, L_c and C_c are chosen once the sensing part is designed.

$$C_{SENS} = \frac{1}{L_c * \left(2\pi * f_{SENSx}\right)^2} - C_c \tag{9}$$

An I^{2}C interface is used for the digital communication with a microcontroller.

IV. Sensing subsystem manufacturing and validation

The sensing subsystem is manufactured using a four layer PCB prototype FR-4 TG130, whose dielectric constant is $\epsilon_r = 4.29$ and thickness $h = 0.36\,\mathrm{mm}$, where circuits are protected by a solder mask ($\epsilon_r = 3.55$), as shown in Figure 5. For real deployments, for further protection, a transparent polyurethane conformal coating is applied ($\epsilon_r = 3.6$). The circuital part of the sensor is protected by encapsulating it in a 3D printed plastic box, filled with epoxy resin, as shown in Figure 12b.

The sensor capacitance on each surface depends on the geometry and thickness of the electrodes, the distance between two adjacent electrodes, the number of electrodes and the material used as dielectric.

Hence, simulations were run to compute the sensing capacitance as a function of w and s, for both the dry and wet case. Results are represented in Figure 6a and Figure 6b, respectively. The choice of smaller values of s and w offers better dynamic, but it requires higher manufacturing costs. For this reason, a trade-off has been chosen: $w = s = 6\,\mathrm{mil}$. Subsequently, few samples were manufactured and simulations were done, considering the presence of solder mask and coating, modelled as a unique dielectric, as they are almost identical ϵ_r.

The capacitance was measured using a digital capacitance meter, connected to the terminals of the sensing unit, and results are represented in Table I, showing an excellent agreement.

Compared to values reported in Figure 6a and Figure 6b, the presence of solder mask and coating reduces the dynamic, so the conditioning circuit can be dimensioned using the wider range of Figure 6a and Figure 6b without limiting the acquisition. In particular, we chose $L_c = 10\,\mu\mathrm{H}$, $C_c = 15\,\mathrm{pF}$. Considering these values, based on the fact that the capacitance cannot be lower than the value of the dry case or higher than the wet case, according to the simulated overall minimum and maximum capacitance, the corresponding frequency range is 500 kHz - 2,7 MHz, which correctly belongs to the FDC2112 one.

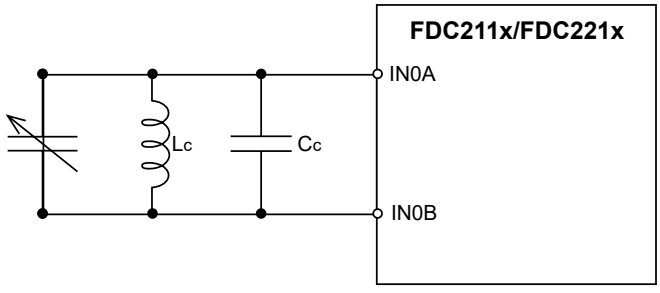

Figure 4: Sensor configuration [11]

Table I: Comparison between simulated and measured capacitance of 3 different PCB samples with solder mask.

Capacitance/sample	PCB #1	PCB #2	PCB #3
Simulated C [pF]	611		
Top C [pF]	625	636	623
Down C [pF]	609	628	636

Figure 5: Final PCB with solder mask, modified from [11]

Sensors characterization was carried out in facilities of Allemano Metrology [18], in a controlled environment using the humidity generator system Thunder 2500 from Thunder Scientific (Figure 7). The UNI CEI EN ISO / IEC 17025:2018 was applied.

An Arduino platform was used to program a microcontroller in order to read the digital output of the CDC, constructing calibration curves.

At first, the capacitance was measured in a climatic chamber, able to ensure fixed temperature and relative humidity (Table II). Subsequently, the samples were immersed in a volume of distilled and deionized water, as shown in Table III and Figure 8.

Results obtained in condition 1 and 2 are similar, with a discrepancy of the mean values of 1.13 pF for the top layer and 2.10 pF for the bottom layer, demonstrating that the sensing output does not depend on relative humidity. Results obtained in condition 3 and 4 are again similar (2.77 pF of discrepancy of the mean values on the top, 3.22 pF on the bottom side of the leaf), demonstrating that it is not necessary to test the device in climatic chamber. Results obtained in condition 5 and 6 demonstrate the linearity of the curve to dew percentage exposure and the absolute difference between capacitances obtained in these conditions is around 0.11 pF. Results obtained in conditions 3 and 7 demonstrate the absence

Table II: Measurements conditions, part I

Condition N°	Testing environment	Temperature [°C]	Relative Humidity [%RH]	Time [s]
1	ad hoc chamber	23.0 ± 0.5	11.0 ± 2.0	1
2	ad hoc chamber	23.0 ± 0.5	95.0 ± 2.0 condition does not cause dew	1
3	ad hoc chamber	0.0 ± 1.0	stable condition of saturation with formation of dew	1

Table III: Measurements conditions, part II

Condition N°	Testing environment	Temperature [°C]	Percentage of immersion volume [%]	Time [s]
4	volume of distilled and deionized water	room	100	1
5	volume of distilled and deionized water	room	50	1
6	volume of distilled and deionized water	room	50 (90° clockwise rotation)	1
7	volume of distilled and deionized water	room	100	3600

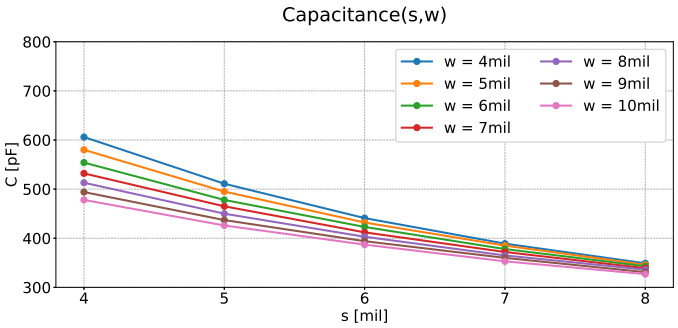

(a) Dry leaf surface

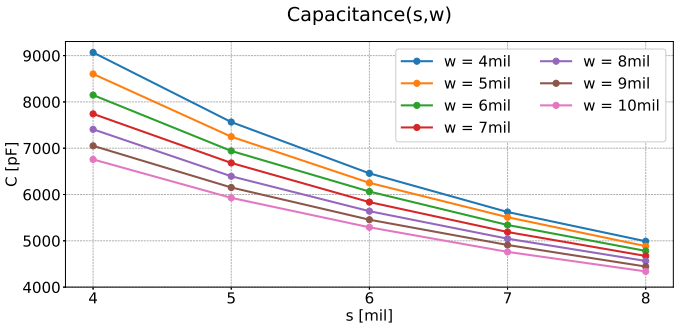

(b) Wet leaf surface

Figure 6: Sensor Capacitance vs s with varying w

Figure 7: Ambient chosen for the LWS characterization [11]

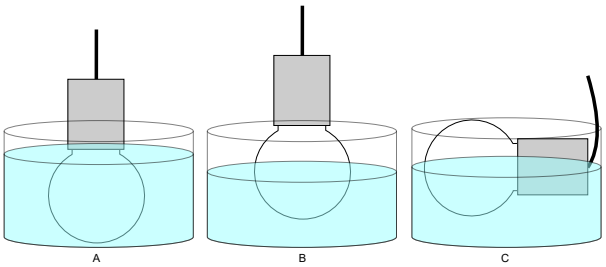

Figure 8: From left to right: (A) Condition 4, (B) Condition 5, (C) Condition 6

of significant drift phenomena (around 3 pF of difference between the beginning and ending of immersion).

Using a volume of distilled and deionized water, 12 sensing units were measured in 4 different conditions: partially immersed for 25%, 50% and 75% and totally immersed. For the repetition of each measuring point, sensors were subjected to complete drying by keeping them at the temperature of 36 °C and relative humidity of 10%. Results are reported in Figure 9.

V. Energy consumption estimate

The energy consumption was measured by means of the AM 503B current probe amplifier [19], which allows to use one probe to simultaneously measure AC and DC currents, with high sensitivity and one-button for autobalancing and probe degaussing. The Amplifier converts the sensed current into a proportional voltage signal, that can be measured directly with an oscilloscope. Figure 11a shows the measured power consumption converted to milliwatt, with the following setting:

- oscilloscope at $10\,\mathrm{mV/DIVISION}$;
- current division of the current probe amplifier set to $10\,\mathrm{mA/DIV}$;
- power source at $3\,\mathrm{V}$.

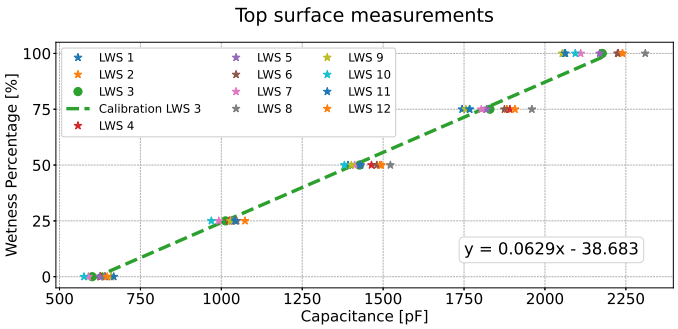

Figure 9: Top surface average measurements of 12 LWSs and example of calibration function for LWS 3

Figure 10: Current Probe Amplifier used to measure the energy consumption

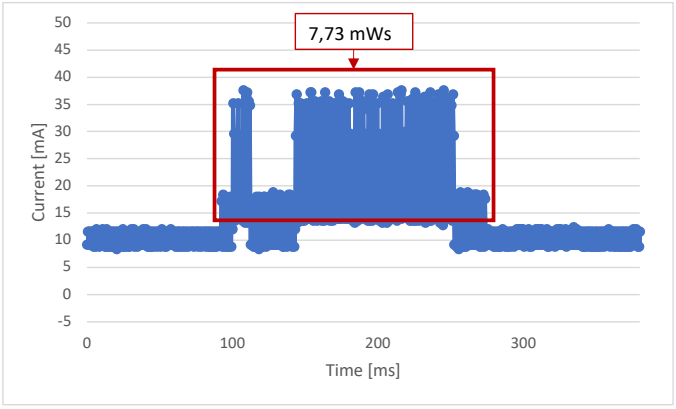

(a) Energy consumption of LWS without boost

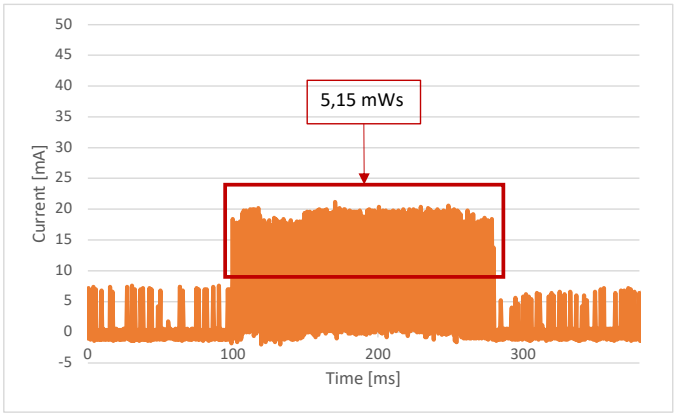

(b) Energy consumption of LWS with boost

Figure 11: Energy consumption of LWS, applying a power source of 3 V

The energy consumption computed with the integral over the period of time of the CDC measurement gives a result of 7.73 mWs.

To further optimize the power consumption of the FDC during the measurement, the output voltage is regulated by means of a switching boost regulator together with a voltage level translator that allows to keep the voltage closer to the desired level without excessive energy expenditure.

The same measuring setting was applied to the sensor with boost (Figure 11b), with current division set to 5 mA/DIV. The presence of the boost lowers the energy in the same time window, even though the current level during the idle period of the CDC is higher than the case without boost, due to the energy consumed by the boost itself. The energy consumption computed with the integral over the time period of a CDC measurement gives a results of 5.15 mWs.

(a)

(b) [11]

Figure 12: Examples of deployment of the LWS within the crop; the LWS simulates the behaviour of the leaf among the real leaves and grapes.

VI. Results

The sensors deployed for the initial investigation during spring 2023 [11] have been maintained for the whole year, allowing to test the new technology during the whole vegetative season, specifically from early March 2023 to late October 2023. Each sensor was installed in a real crop(Figure 12, connected to a custom board exploited to perform and store a measure every 10 minutes. The board implements an STMicroelectronics microcontroller STM32L0 and a Semtech LoRa radio SX1272, all powered by two AA alkaline batteries in series.

Tests proved that our sensor is capable to operate in a real environment for at least an entire season; only 20% of the batteries was consumed.

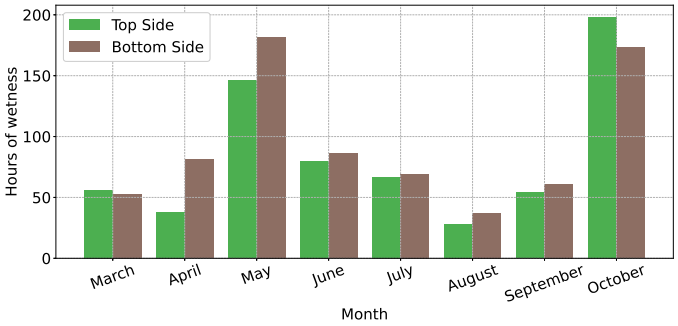

(a) Leaf wetness hours per month

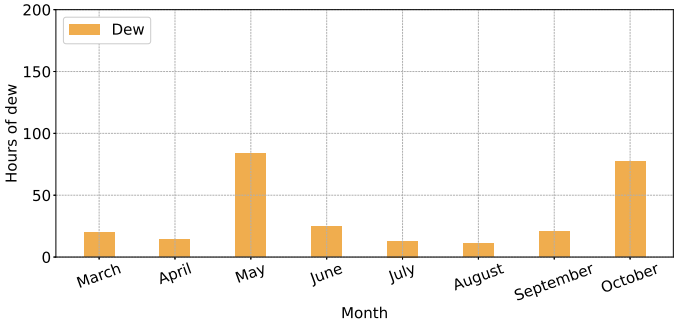

(b) Dew hours per month

Figure 13: Measurements over the period March - October 2023

The seasonal results can be seen in Figure 13a, where the total amount of hours of leaf wetness higher than 50% is reported for each month. Instead, Figure 13b represents the hours of dew per month, during the same season, measured by an air humidity and temperature sensor. The dew point has been computed and compared with the temperature in order to evaluate the presence of dew, i.e. when temperature and dew point are very close. Similar trends are found in both histograms, which confirms the good quality of the measures acquired, but the leaf wetness sensor globally records more wetness hours with respect to the indirect measurement.

Multiple reasons can explain this behavior. First of all, the leaf wetness is not only caused by dew, but also by other phenomena, for example the evapotranspiration that releases water vapor from the soil to the atmosphere or more simply rainfalls. In this case, the dew point alone may be not accurate enough to estimate the leaf wetness, as previously explained in [11].

An example of this phenomenon can be seen in Figure 14, where a detailed overview of the period August 28th - 31th is shown. At the very beginning, a rainfall event (Figure 14c) was registered with a subsequent increase of the volumetric water content of the soil (Figure 14d). After that, leaf wetness was detected, which was not known with the dew point information alone, since the two curves of temperature and dew point are too distant between each other in Figure 14b. It is noteworthy that the bottom layer of the leaf was more susceptible to this event than the top layer, confirming that measuring both the layers remains an important aspect for the overall estimation of leaf wetness.

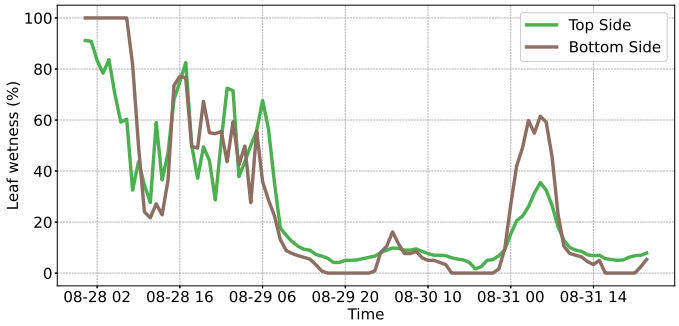

(a) Leaf wetness

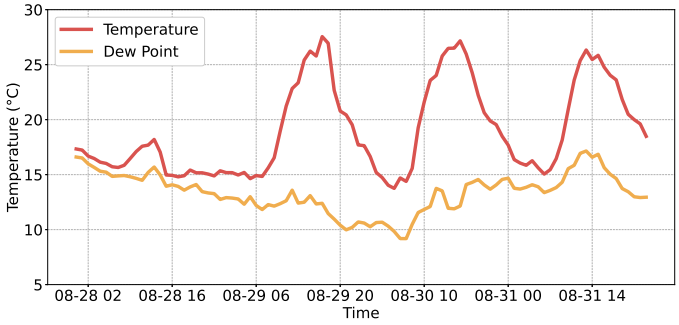

(b) Temperature and dew point

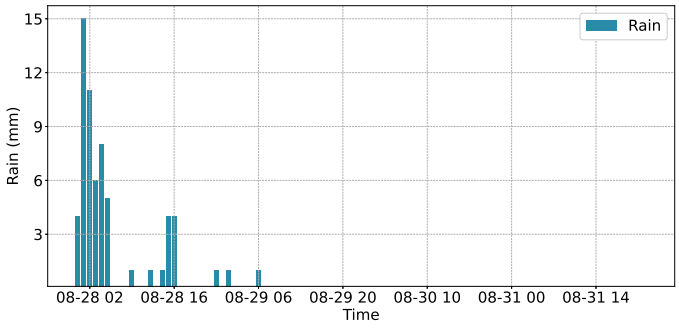

(c) Rain

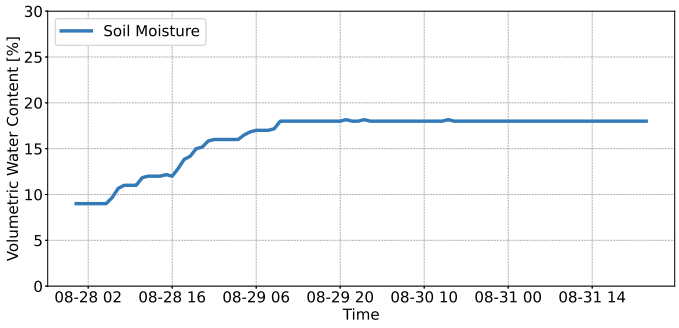

(d) Soil Moisture

Figure 14: LWS detecting special wetness caused by past rain falls

VII. Conclusion

This work shows the full design process for the leaf wetness sensor, involving both sensing and data acquisition subsystems.

The choice of a capacitive measurement allows the characterization of the percentage of leaf surface exposed to wetness, while resistive solutions cannot discriminate it. Solutions like

the ones reported in [7] and [8] are less optimized, as they do not implement the whole sensor in a unique board. Differently from those ones, our solution is more compact and simpler, leading to optimized energy efficiency. The usage of a dedicated CDC, compared to solutions implementing a generic microcontroller, is more efficient energetically [9]. Other solutions like [10], based on microwave implementation, are more precise, but big in dimensions and require much higher power. Our sensor, moreover, is able to distinguish between what occurs on the upper and the lower sides, with a capacitor reader integrated on board and totally energetically optimized.

The overall results demonstrate the quality and stability of the device, which is capable to outperform classic indirect leaf wetness estimation techniques.

Tests in laboratory and on the field prove that the proposed sensor can be exploited in IoT applications, thanks to the low energy consumption.

The current configuration is potentially limited. As it is designed, when configured as a sensing unit of a wireless sensor node, the proposed sensor needs a wired connection to the node microcontroller. This wire can be damaged by severe weather conditions, animals or accidental agronomic activities. For this reason, the integration of a microcontroller, radio, antenna and power supply on the same board used to manufacture the sensor should be considered for future applications.

Acknowledgment

The authors would like to thank Allemano Metrology Srl for the support and the instrumentation necessary for the test and the calibration process.

References

[1] CE Yarwood. “Water and the infection process”. In: *Water and plant disease* 5 (1978), pp. 141–173.

[2] A. Ghobakhlou, F. Amir, and P. Sallis. “Leaf wetness sensors - a comparative analysis”. In: *2015 9th International Conference on Sensing Technology (ICST)*. 2015, pp. 420–424. DOI: 10.1109/ICSensT.2015.7438434.

[3] Tracy Rowlandson et al. “Reconsidering Leaf Wetness Duration Determination for Plant Disease Management”. In: *Plant Disease* 99 (Mar. 2015), pp. 310–319. DOI: 10.1094/PDIS-05-14-0529-FE.

[4] Rodger Getz. *Report on the measurement of leaf wetness*. World Meteorological Organization, 1992.

[5] Paulo C. Sentelhas et al. “Suitability of relative humidity as an estimator of leaf wetness duration”. In: *Agricultural and Forest Meteorology* 148.3 (2008), pp. 392–400. ISSN: 0168-1923. DOI: https://doi.org/10.1016/j.agrformet.2007.09.011. URL: https://www.sciencedirect.com/science/article/pii/S0168192307002614.

[6] JULIUS F. BOSEN. “AN APPROXIMATION FORMULA TO COMPUTE RELATIVE HUMIDITY FROM DRY BULB AND DEW POINT TEMPERATURES”. In: *Monthly Weather Review* 86.12 (1958), pp. 486–486. DOI: https://doi.org/10.1175/1520-0493(1958)086⟨0486:AAFTCR⟩2.0.CO;2. URL: https://journals.ametsoc.org/view/journals/mwre/86/12/1520-0493_1958_086_0486_aaftcr_2_0_co_2.xml.

[7] Kamlesh S. Patle et al. “IoT Enabled, Leaf Wetness Sensor on the Flexible Substrates for In-Situ Plant Disease Management”. In: *IEEE Sensors Journal* 21.17 (2021), pp. 19481–19491. DOI: 10.1109/JSEN.2021.3089722.

[8] Shahid Malik et al. “A Fringing Field Based Screen-Printed Flexible Capacitive Moisture and Water Level Sensor”. In: *2020 IEEE International Conference on Flexible and Printable Sensors and Systems (FLEPS)*. 2020, pp. 1–4. DOI: 10.1109/FLEPS49123.2020.9239552.

[9] Gemma Hornero et al. “A novel low-cost smart leaf wetness sensor”. In: *Computers and Electronics in Agriculture* 143 (2017), pp. 286–292. ISSN: 0168-1699. DOI: https://doi.org/10.1016/j.compag.2017.11.001. URL: https://www.sciencedirect.com/science/article/pii/S0168169917305197.

[10] Elisa Pievanelli, Riccardo Stefanelli, and Daniele Trinchero. “Microwave-based leaf wetness detection in agricultural wireless sensor networks”. In: *2016 IEEE Sensors Applications Symposium (SAS)*. 2016, pp. 1–4. DOI: 10.1109/SAS.2016.7479881.

[11] Elena Filipescu, Giovanni Paolo Colucci, and Daniele Trinchero. “Advances in Design and Construction of Leaf Wetness Sensors”. In: *2023 IEEE Conference on AgriFood Electronics (CAFE)*. 2023, pp. 128–131. DOI: 10.1109/CAFE58535.2023.10291759.

[12] F. H. Drake, G. W. Pierce, and M. T. Dow. “Measurement of the Dielectric Constant and Index of Refraction of Water and Aqueous Solutions of KCl at High Frequencies”. In: *Physical Review* 35.6 (Mar. 1930), pp. 613–622. DOI: 10.1103/PhysRev.35.613.

[13] G. Ghione and C. Naldi. “Parameters of coplanar waveguides with lower ground plane”. In: *ELECTRONIC LETTERS* 19 (Sept. 1983), pp. 734–735. DOI: 10.1049/el:19830500.

[14] Brian C Wadell. *Transmission line design handbook / Brian C. Wadell*. eng. Artech House microwave library. Boston London: Artech House, 1991.

[15] M. Riaziat et al. “SINGLE-MODE OPERATION OF COPLANAR WAVEGUIDES”. eng. In: *Electronics letters* 23.24 (1987), pp. 1281–1283. ISSN: 0013-5194.

[16] *FDC2x1x EMI-Resistant 28-Bit,12-Bit Capacitance-to-Digital Converter for Proximity and Level Sensing Applications*. SNOSCZ5A. Rev. A. Texas Instruments. June 2015.

[17] *FDC1004 4-Channel Capacitance-to-Digital Converter for Capacitive Sensing Solutions*. SNOSCY5B. Rev. B. Texas Instruments. Apr. 2015.

[18] URL: https://www.allemanometrology.com/wp/.

[19] *AM 503B & AM 5030 AC/DC Current Probe Amplifiers*. 070-8766-05. Instruction Manual. Tektronix.